

## Electrocatalysis

International Edition: DOI: 10.1002/anie.201708748  
German Edition: DOI: 10.1002/ange.201708748MoB/g-C<sub>3</sub>N<sub>4</sub> Interface Materials as a Schottky Catalyst to Boost Hydrogen EvolutionZechao Zhuang<sup>+</sup>, Yong Li<sup>+</sup>, Zilan Li<sup>+</sup>, Fan Lv, Zhiquan Lang, Kangning Zhao, Liang Zhou, Lyudmila Moskaleva,\* Shaojun Guo,\* and Liqiang Mai\*

**Abstract:** Proton adsorption on metallic catalysts is a prerequisite for efficient hydrogen evolution reaction (HER). However, tuning proton adsorption without perturbing metallicity remains a challenge. A Schottky catalyst based on metal–semiconductor junction principles is presented. With metallic MoB, the introduction of n-type semiconductive g-C<sub>3</sub>N<sub>4</sub> induces a vigorous charge transfer across the MoB/g-C<sub>3</sub>N<sub>4</sub> Schottky junction, and increases the local electron density in MoB surface, confirmed by multiple spectroscopic techniques. This Schottky catalyst exhibits a superior HER activity with a low Tafel slope of 46 mV dec<sup>-1</sup> and a high exchange current density of 17 μA cm<sup>-2</sup>, which is far better than that of pristine MoB. First-principle calculations reveal that the Schottky contact dramatically lowers the kinetic barriers of both proton adsorption and reduction coordinates, therefore benefiting surface hydrogen generation.

Hydrogen is undeniably pursued as one of the most promising green energy carriers to meet sustainability imperatives.<sup>[1]</sup> Molybdenum-based electrocatalysts (such as MoS<sub>2</sub>, Mo<sub>2</sub>C, MoO<sub>2</sub>, MoP, and MoB) are emerging as a promising class of noble metal-free catalysts for HER in both acid and alkaline media.<sup>[2]</sup> Strongly dependent on their electron and phonon structures, Mo-based catalysts exhibit a moderate “Pt-like” hydrogen binding energy on catalytic centers and a metallic-like transport nature in solid.<sup>[3]</sup> Thus, it is widely

accepted that further optimization of their catalytic performance lies in more precise tuning of the electron and phonon behaviors.<sup>[3,4]</sup> Many advances have been reported during the last decade, including creating vacancies,<sup>[3c,5]</sup> phase transformation,<sup>[3b,4a,6]</sup> or band engineering,<sup>[4b,7]</sup> which successfully endow additional active sites to Mo-based catalysts for boosting HER catalysis. However, these tactics often inevitably alter the electron transport property at the same time. In particular, the excessively introduced defects may disorder the primitive lattice and induce the anisotropic scattering of phonons, leading to sharp decreases in electron transport efficiency and loss of activity.<sup>[3c,8]</sup> Given this, an effective strategy for catalyst surface modulation without perturbing interior conductivity is urgently required.

A Schottky junction, formed at the metal–semiconductor interface, is usually introduced to generate the built-in electric field and enhance the charge separation and transportation for the operation of many semiconductor devices. The difference in Fermi levels between metal and semiconductor sides drives the charge flow propagated by electrons or holes until the system reaches equilibrium, followed by band bending and Schottky barrier formation (Figure 1). Rational selection of a semiconductor with suitable majority-carrier type and band structure to build a delicate Schottky junction can adjust the surface charge density of metallic catalyst for specific catalytic reactions.<sup>[9,10]</sup> For cathodic HER, a metallic surface with enriched electron density could lead to the stabilization of adsorbed hydrogen and catalytic activity enhancement.<sup>[2,3]</sup> In this regard, designing an ingenious Mo-based Schottky catalyst to achieve more efficient HER, without introducing new lattice defects, is highly desirable, but still waiting to be developed.

[\*] Z. Zhuang,<sup>[+]</sup> Z. Li,<sup>[+]</sup> Z. Lang, K. Zhao, Prof. L. Zhou, Prof. L. Mai  
State Key Laboratory of Advanced Technology for Materials Synthesis and Processing, International School of Materials Science and Engineering, Wuhan University of Technology  
Wuhan 430070 (China)  
E-mail: mlq518@whut.edu.cn

F. Lv, Prof. S. Guo  
Department of Materials Science and Engineering  
College of Engineering, Peking University  
Beijing 100871 (China)  
E-mail: guosj@pku.edu.cn

Y. Li,<sup>[+]</sup> Dr. L. Moskaleva  
Institute of Applied and Physical Chemistry and Center for Environmental Research and Sustainable Technology, Universität Bremen  
28359 Bremen (Germany)  
E-mail: moskaleva@uni-bremen.de

Prof. L. Mai  
Department of Chemistry, University of California  
Berkeley, CA 94720 (USA)

[†] These authors should be considered as co-first authors.

Supporting information and the ORCID identification number(s) for the author(s) of this article can be found under:  
<https://doi.org/10.1002/anie.201708748>.

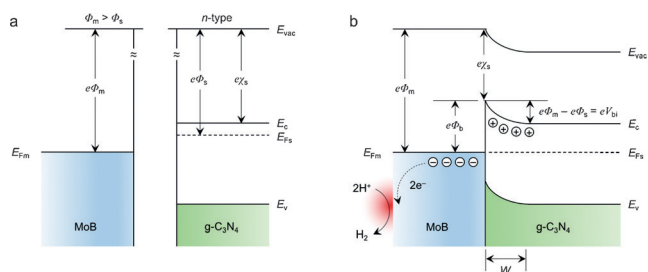


**Figure 1.** Energy band diagrams of metallic MoB and n-type semiconductive g-C<sub>3</sub>N<sub>4</sub> before (a) and after Schottky contact (b). E<sub>vac</sub> = vacuum energy, E<sub>c</sub> = conduction band, E<sub>v</sub> = valence band, E<sub>F</sub> = Fermi level, Φ = vacuum electrostatic potential, χ = vacuum ionization energy, V = electric potential, e = electric charge, W = depletion region.

Herein, we report a MoB/g-C<sub>3</sub>N<sub>4</sub> Schottky catalyst with remarkable HER activity enhancement by inducing the charge redistribution across a Schottky contact with an n-type semiconductor. Tetragonal  $\alpha$ -MoB, displaying intrinsic metallicity, is chosen as our paradigm, and proposed as an alternative HER catalyst (yielding Tafel slopes of about 60 mV dec<sup>-1</sup>).<sup>[2f,g,11]</sup> We utilize an n-type g-C<sub>3</sub>N<sub>4</sub> with a wide band gap of 2.7 eV as the semiconductor side. The Fermi level of g-C<sub>3</sub>N<sub>4</sub> outbalances substantially all metals, and makes itself available for Schottky contact formation.<sup>[12]</sup> A series of MoB/g-C<sub>3</sub>N<sub>4</sub> Schottky catalysts with diverse charge-transfer states were simply constructed by proportionally blending two components. As expected, the optimal Schottky catalyst exhibits an outstanding and stable performance with a Tafel slope of 46 mV dec<sup>-1</sup> and an exchange current density of 17  $\mu$ A cm<sup>-2</sup>, which is far better than that of pristine MoB. Such a synergistic optimization is clearly understood by integrating spectroscopic evidence with theory computations. This study embraces the band theory and provides an accessible method to activate metallic Mo-based catalysts.

Figure 2a shows the X-ray diffraction (XRD) pattern of commercial MoB. It can be indexed to a tetragonal structure in space group  $I4_1/amd$  ( $Z=8$ ), in which alternate zigzag chains of boron atoms align along the [100] and [010] crystallographic directions, and each boron chain is enclosed by hexagonal molybdenum atoms (inset of Figure 2a). A metallic temperature-dependent resistivity for MoB is observed as anticipated (Figure 2b), manifesting an increase of resistance in signal with increasing temperature within the whole measured range of 20–300 K. Density functional theory (DFT) calculation also reveals the intrinsic metallicity of MoB with large local density of states (DOS) across the Fermi level (Supporting Information, Figure S1). The XRD pattern of as-prepared g-C<sub>3</sub>N<sub>4</sub> in Figure 2c displays two typical (100)

and (002) diffraction peaks, providing a solid evidence for the successful formation of g-C<sub>3</sub>N<sub>4</sub>. The C/N molar ratio is close to the theoretical value of about 0.75, determined by X-ray photoelectron spectroscopy (XPS) and elemental combustion analysis (Supporting Information, Figure S2). The band gap energy of g-C<sub>3</sub>N<sub>4</sub> is further calculated to be about 2.7 eV using Kubelka–Munk remission function (Figure 2d and its inset), being in accordance with the previous reports.<sup>[12,13]</sup> To fabricate an effective Schottky junction (Figure 1), the proportional quantities of both samples were mixed and ground. The scanning electron microscopy (SEM) and transmission electron microscopy (TEM) images of the mixture, coupled with energy-dispersive spectroscopy (EDS) elemental mapping, demonstrate that the Mo, B, C, and N signals spatially correlate with each other, indicating the close mutual contacts between the powder samples (Supporting Information, Figures S3 and S4). Meanwhile, the crystallinity of MoB and g-C<sub>3</sub>N<sub>4</sub> after mixing remains unchanged, and no contamination was introduced (Supporting Information, Figure S5).

The HER activities of MoB, g-C<sub>3</sub>N<sub>4</sub>, and MoB/g-C<sub>3</sub>N<sub>4</sub> Schottky catalysts were examined in N<sub>2</sub>-saturated 1M KOH solution. The linear sweep voltammetry (LSV) curve of the pristine MoB shows an onset overpotential of about 80 mV (Figure 3a), while the semiconductive g-C<sub>3</sub>N<sub>4</sub> does not show an obvious HER activity (Supporting Information, Figure S6). For MoB/g-C<sub>3</sub>N<sub>4</sub> Schottky catalyst, its voltammogram presents an obvious shift to a more positive overpotential of about 40 mV, beyond which the cathodic current rises steeply along negative potentials. This Schottky catalyst attains a cathodic current of 20 mA cm<sup>-2</sup> at the overpotential of 152 mV, whereas the pristine MoB only reaches about 4 mA cm<sup>-2</sup> under the same condition. The Tafel plots and exchange current densities were also extracted (Figure 3b;

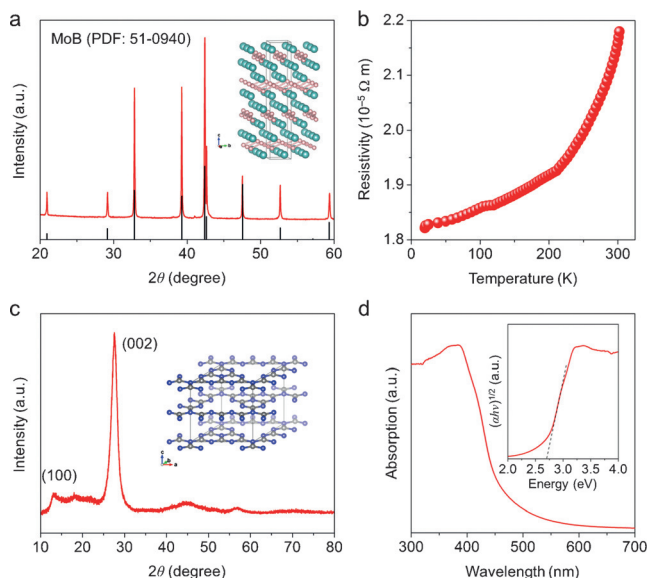


**Figure 2.** a) XRD pattern and b) temperature-dependent resistivity ( $\rho$ - $T$ ) plots for commercial MoB powders. c) XRD pattern and d) UV/Vis analysis for g-C<sub>3</sub>N<sub>4</sub> powders. Insets show corresponding crystal structures in (a) and (b).

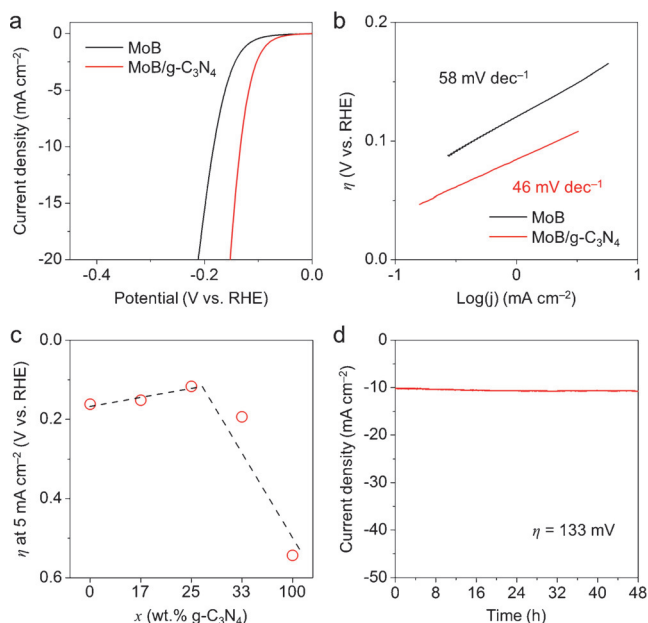


**Figure 3.** a) LSV polarization curves and b) corresponding Tafel plots. c) A volcano-shaped plot of overpotentials at 5 mA cm<sup>-2</sup> with respect to MoB/g-C<sub>3</sub>N<sub>4</sub> Schottky catalysts with different weight ratios. d) Chronoamperometric current–time ( $i$ - $t$ ) tests.

Supporting Information, Table S1). The pristine MoB displays a Tafel slope of  $58 \text{ mV dec}^{-1}$  and an exchange current density of  $8 \mu\text{A cm}^{-2}$ . Rather, the MoB/g- $\text{C}_3\text{N}_4$  Schottky catalyst shows a far higher HER activity with a lower Tafel slope of  $46 \text{ mV dec}^{-1}$  and a higher exchange current density of  $17 \mu\text{A cm}^{-2}$ , comparable to, or even exceeding those state-of-the-art noble metal-free catalysts (Supporting Information, Table S1). Additionally, the Tafel slope of the MoB/g- $\text{C}_3\text{N}_4$  close to about  $40 \text{ mV dec}^{-1}$  indicates that electrochemical surface desorption of adsorbed hydrogen, namely Heyrovsky reaction, should strongly control the HER process.<sup>[14]</sup> The electrochemical impedance spectroscopy (EIS) plots (Supporting Information, Figure S7) show that the MoB/g- $\text{C}_3\text{N}_4$  possesses a much smaller  $R_{ct}$  than the pristine MoB, indicating a faster HER dynamics involved. The activity of this system shows a volcano-shaped dependence on composition ratios (Figure 3c), which illustrates that only an appropriate amount of g- $\text{C}_3\text{N}_4$  can lead to the maximum synergistic effect. Moreover, a similar trend for activity improvement was also observed in an acid solution (Supporting Information, Figure S6). Such a trend originates from the fact that introducing excessive inert g- $\text{C}_3\text{N}_4$  suppresses the positive Schottky effects. Furthermore, the HER performance observed in alkaline media is higher than that in the acid counterpart. This trend may stem from the fact that the Lewis acidity of boron favors the adsorption of  $\text{OH}^-$  ions, and the rate-limiting water dissociation of alkaline HER. The effects of carbon Vulcan XC72R and hand grinding on HER activity was explored. The results further reveal the major factor in enhancing HER activity of MoB/g- $\text{C}_3\text{N}_4$  is indeed caused by Schottky contact (Supporting Information, Figures S8–S10 and Table S2).

Long-term durability is another key requirement for HER catalysts in industrial applications. The catalysts were analyzed through a chronoamperometric test (Figure 3d; Supporting Information, Figure S11). At a fixed overpotential of 133 mV, the MoB/g- $\text{C}_3\text{N}_4$  Schottky catalyst yields a stable current density of about  $10 \text{ mA cm}^{-2}$  over 48 h (Figure 3d), similar to the pristine MoB, which also exhibits a stable HER performance but at a much higher overpotential of 183 mV (Supporting Information, Figure S11). Continuous cyclic voltammetry (CV) was also employed to evaluate the durability of MoB/g- $\text{C}_3\text{N}_4$ . It shows a negligible loss of cathodic current after 5000 cycles, further indicating its high stability for HER (Supporting Information, Figure S12).

A number of spectroscopic techniques, combined with first-principles simulations, were used to investigate the interfacial interactions and electronic structures of metal and semiconductor before and after Schottky contact. Figure 4a shows XPS spectra of MoB and MoB/g- $\text{C}_3\text{N}_4$ . A negative shift (ca. 0.4 eV) of typical Mo  $3d_{5/2}$  XPS peaks is observed on MoB/g- $\text{C}_3\text{N}_4$ . And also other Mo XPS peaks, attributed to thin surface oxide, were also shifted negatively on MoB/g- $\text{C}_3\text{N}_4$  (Supporting Information, Figure S13). Generally, binding energy negatively correlates with surface electron density.<sup>[15]</sup> The XPS results suggest that the electrons donated from g- $\text{C}_3\text{N}_4$  are enriched on the MoB surface. Besides the Mo element, the electron density of B was also increased after Schottky contact with g- $\text{C}_3\text{N}_4$  (Supporting Information, Figure S14). The energy-loss near-edge struc-

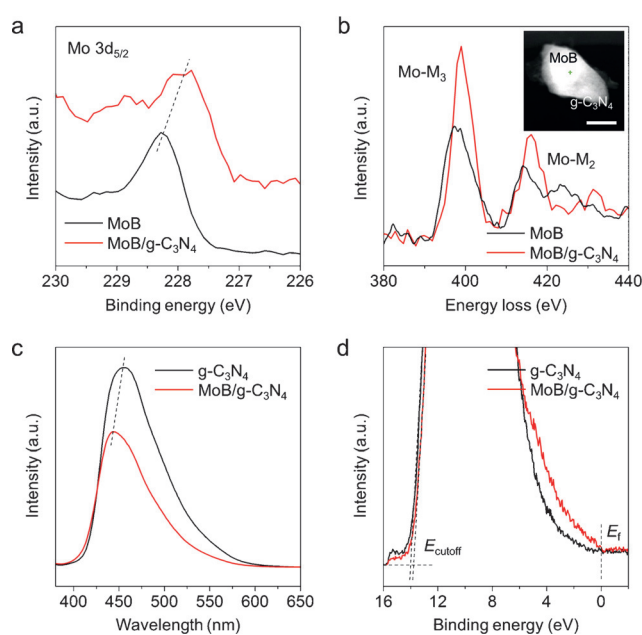


**Figure 4.** a) Mo  $3d_{5/2}$  XPS spectra and b) ELNES of Mo- $M_{2,3}$  edges for pure MoB and MoB/g- $\text{C}_3\text{N}_4$  Schottky catalyst. c) PL spectra and d) UPS analysis for pure g- $\text{C}_3\text{N}_4$  and MoB/g- $\text{C}_3\text{N}_4$  Schottky catalyst. Inset shows corresponding high-angle annular dark field (HAADF) image with, green “+” indicating the selected region for EELS analysis. Scale bar: 50 nm.

tures (ELNES) spectra of Mo- $M_{2,3}$  edges, which behave sensitively with stimulated 3p electron transitions from spin-orbit-split states to quasi-localized states and reflect the local environment of Mo, are shown in Figure 4b. Clearly, the edge-onsets of both the  $M_3$  and  $M_2$  peaks move toward higher energy losses by about 2 eV after Schottky contact (inset of Figure 4b), implying the alterations in the electronic state of Mo atoms. The  $M_3/M_2$  intensity ratios were found to be 1.5 and 1.8 for MoB and MoB/g- $\text{C}_3\text{N}_4$ , respectively. These ELNES results further support that the Schottky effect creates a fraction of Mo atoms in a reduced state, in decent agreement with the XPS results.

Next, photoluminescence (PL) and ultraviolet photoemission spectroscopy (UPS) were applied to confirm the interface state and band alignments of g- $\text{C}_3\text{N}_4$ . A blue-shifted emission peak was observed in the PL spectrum of the MoB/g- $\text{C}_3\text{N}_4$  Schottky catalyst (Figure 4c), indicating a band gap widening, as the electron depletion causes an upshifting of conduction band edge of g- $\text{C}_3\text{N}_4$ .<sup>[16]</sup> Further, its PL quenching suggests that the electron–hole pair recombination in the semiconductive g- $\text{C}_3\text{N}_4$  is suppressed and thus the charge separation is enhanced<sup>[16b]</sup> because the excited electrons are readily trapped by metallic MoB. UPS analysis was used to scrutinize the variations in the work function of g- $\text{C}_3\text{N}_4$ . Figure 4d depicts the UPS spectra with the cutoff energy ( $E_{\text{cutoff}}$ ) regions at high binding energies. The  $E_{\text{cutoff}}$  of g- $\text{C}_3\text{N}_4$  and MoB/g- $\text{C}_3\text{N}_4$  is 13.9 eV and 13.7 eV, respectively, while the  $E_f$  is 0 eV in both cases. The corresponding work functions ( $e_\phi$ ) can be estimated to be 7.3 eV and 7.5 eV according to the following equation,  $e_\phi = h\nu - |E_{\text{cutoff}} - E_f|$ .<sup>[17]</sup> Such an upshift (ca. 0.2 eV) of the work function validates again the existing

Schottky effect. The same conclusion can be further proved by analyzing the spatial charge density difference on a periodic slab model of MoB/g-C<sub>3</sub>N<sub>4</sub> (Supporting Information, Figure S15). As shown in Figure 5a,b, the charge density of the junction interface is plainly redistributed after the contact between MoB and g-C<sub>3</sub>N<sub>4</sub>, forming a negatively charged MoB surface and a positively charged g-C<sub>3</sub>N<sub>4</sub>. This computed geometry corroborates the presence of Schottky junction with vigorous electron transfer from g-C<sub>3</sub>N<sub>4</sub> to MoB.

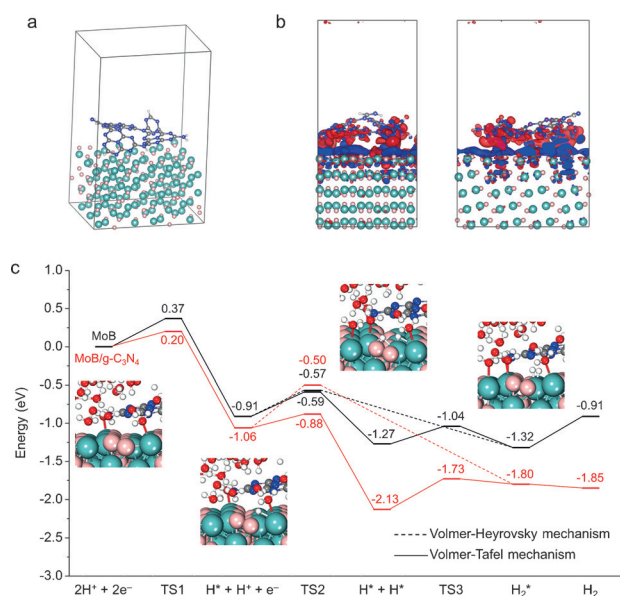


**Figure 5.** a) Periodic slab model of MoB(112)/g-C<sub>3</sub>N<sub>4</sub> Schottky catalyst and its b) spatial charge density difference isosurfaces. Blue and red isosurfaces represent electron accumulation and electron depletion, respectively. c) Energy profiles of HER on pure MoB and MoB/g-C<sub>3</sub>N<sub>4</sub> Schottky catalyst.

To further provide atomic- and molecular-level understandings, we calculated the detailed energy profiles of HER pathways on bare MoB and MoB/g-C<sub>3</sub>N<sub>4</sub> catalysts (Figure 5c). Considering that MoB (112) facet has the highest exposure percentage in MoB, we therefore chose this surface as our DFT model example. The strongly coupled Mo–B atoms on the MoB surface are well established as the active site,<sup>[18]</sup> thermodynamically capable of catalyzing the two-electron reduction of two protons to yield dihydrogen. The reaction pathway primarily involves proton adsorption and reduction on the catalyst surface, followed by chemical or electrochemical desorption of the hydrogen molecule. Two possible mechanisms are generally accepted, namely Volmer–Tafel and Volmer–Heyrovsky, to distinguish the different desorption behaviors. For MoB/g-C<sub>3</sub>N<sub>4</sub>, the overall reaction energies are much lower than those of MoB according to either mechanism. The result demonstrates the higher intrinsic HER activity of this Schottky catalyst and satisfactorily interprets its lower overpotential under a real electrochemical condition. Regarding kinetic barriers, the introduction of g-C<sub>3</sub>N<sub>4</sub> lowers the energy barrier for rate-limiting proton adsorption on the MoB by 0.17 eV in the first Volmer

step, guaranteeing abundant coverage of adsorbed hydrogen on the catalyst surface for the following steps. If HER further proceeds according to Volmer–Tafel route, the following steps include another proton adsorption and recombination. The second proton can also be easily adsorbed onto the MoB/g-C<sub>3</sub>N<sub>4</sub>, while the recombination of two protons with a high barrier of 0.40 eV becomes the new rate-limiting step. In the alternative Volmer–Heyrovsky mechanism, the electrochemical desorption step exhibits a higher energy barrier of 0.56 eV, indicating that the HER on the MoB/g-C<sub>3</sub>N<sub>4</sub> more likely occurs through a Volmer–Tafel route. This finding seems to be in conflict with the experimental results by Tafel slopes, but the fact should be considered that the use of large and irregular MoB particles may hinder the electron and proton transport during HER, leading to a loss of activity. Therefore, we can expect a better activity through downsizing this Schottky catalyst to compensate the imperfection. From the computational point of view, introducing n-type semiconductive g-C<sub>3</sub>N<sub>4</sub> on MoB catalyst indeed creates a situation in which the surface electron density of MoB is enriched such that the proton access to active sites is facilitated, and the reduction kinetic barrier is lowered, significantly boosting the surface hydrogen generation.

In summary, we demonstrate an ingenious strategy to optimize HER catalytic activity of metallic MoB by contacting n-type semiconductive g-C<sub>3</sub>N<sub>4</sub> to form a Schottky junction. This Schottky catalyst exhibits a superior and durable HER performance with a Tafel slope of 46 mV dec<sup>-1</sup> and an exchange current density of 17 μA cm<sup>-2</sup>, far outperforming the pristine MoB. As revealed by spectroscopic studies, the interface between the MoB and g-C<sub>3</sub>N<sub>4</sub> features notable charge redistribution. The activity enhancement can therefore be attributed to the enriched electron density of the MoB surface and to unimpeded electron transfer in the bulk. Computations further validate the lowered kinetic barriers of both proton adsorption and reduction on the Schottky catalyst. This development opens a new avenue for activating metallic electrocatalysts from the band theory of solids.

### Acknowledgements

This work was supported by the National Key Research and Development Program of China (2016YFA0202603), the National Basic Research Program of China (2013CB934103), the Programme of Introducing Talents of Discipline to Universities (B17034), the National Natural Science Foundation of China (51521001, 51671003), the National Natural Science Fund for Distinguished Young Scholars (51425204), the Fundamental Research Funds for the Central Universities (WUT: 2016III001, 2017III009), and the State Key Laboratory of Advanced Technology for Materials Synthesis and Processing (WUT: 2017-KF-2). We thank the North-German Supercomputing Alliance (HLRN) for providing computational resources. Prof. Liqiang Mai gratefully acknowledged financial support from China Scholarship Council (No. 201606955096).

**Conflict of interest**

The authors declare no conflict of interest.

**Keywords:** electrocatalysis · graphitic carbon nitride · hydrogen evolution reaction · molybdenum boride · Schottky junction

**How to cite:** *Angew. Chem. Int. Ed.* **2018**, *57*, 496–500  
*Angew. Chem.* **2018**, *130*, 505–509

- [1] a) Z. W. Seh, J. Kibsgaard, C. F. Dickens, I. Chorkendorff, J. K. Nørskov, T. F. Jaramillo, *Science* **2017**, *355*, eaad4998; b) L. Lin, W. Zhou, R. Gao, S. Yao, X. Zhang, W. Xu, S. Zheng, Z. Jiang, Q. Yu, Y.-W. Li, et al., *Nature* **2017**, *544*, 80–83.
- [2] a) J. Kibsgaard, Z. Chen, B. N. Reinecke, T. F. Jaramillo, *Nat. Mater.* **2012**, *11*, 963–969; b) W.-F. Chen, C.-H. Wang, K. Sasaki, N. Marinkovic, W. Xu, J. T. Muckerman, Y. Zhu, R. R. Adzic, *Energy Environ. Sci.* **2013**, *6*, 943; c) L. Liao, S. Wang, J. Xiao, X. Bian, Y. Zhang, M. D. Scanlon, X. Hu, Y. Tang, B. Liu, H. H. Girault, *Energy Environ. Sci.* **2014**, *7*, 387–392; d) Y. Jin, H. Wang, J. Li, X. Yue, Y. Han, P. K. Shen, Y. Cui, *Adv. Mater.* **2016**, *28*, 3785–3790; e) P. Xiao, M. A. Sk, L. Thia, X. Ge, R. J. Lim, J.-Y. Wang, K. H. Lim, X. Wang, *Energy Environ. Sci.* **2014**, *7*, 2624–2629; f) H. Vruble, X. Hu, *Angew. Chem. Int. Ed.* **2012**, *51*, 12703–12706; *Angew. Chem.* **2012**, *124*, 12875–12878; g) H. Park, A. Encinas, J. P. Scheifers, Y. Zhang, B. P. T. Fokwa, *Angew. Chem. Int. Ed.* **2017**, *56*, 5575–5578; *Angew. Chem.* **2017**, *129*, 5667–5670; h) X. Zhang, H. Cheng, H. Zhang, *Adv. Mater.* **2017**, *29*, 1701704; i) C. Tan, X. Cao, X.-J. Wu, Q. He, J. Yang, X. Zhang, J. Chen, W. Zhao, S. Han, G.-H. Nam, M. Sindoro, H. Zhang, *Chem. Rev.* **2017**, *117*, 6225–6331.
- [3] a) T. F. Jaramillo, K. P. Jorgensen, J. Bonde, J. H. Nielsen, S. Horch, I. Chorkendorff, *Science* **2007**, *317*, 100–102; b) M. A. Lukowski, A. S. Daniel, F. Meng, A. Forticaux, L. Li, S. Jin, *J. Am. Chem. Soc.* **2013**, *135*, 10274–10277; c) H. Li, C. Tsai, A. L. Koh, L. Cai, A. W. Contryman, A. H. Fragapane, J. Zhao, H. S. Han, H. C. Manoharan, F. Abild-Pedersen, et al., *Nat. Mater.* **2016**, *15*, 48–53; d) Q. Lu, Y. Yu, Q. Ma, B. Chen, H. Zhang, *Adv. Mater.* **2016**, *28*, 1917–1933; e) X. Zhang, Z. Lai, C. Tan, H. Zhang, *Angew. Chem. Int. Ed.* **2016**, *55*, 8816–8838; *Angew. Chem.* **2016**, *128*, 8960–8984.
- [4] a) J. Xie, J. Zhang, S. Li, F. Grote, X. Zhang, H. Zhang, R. Wang, Y. Lei, B. Pan, Y. Xie, *J. Am. Chem. Soc.* **2013**, *135*, 17881–17888; b) J. Wang, M. Yan, K. Zhao, X. Liao, P. Wang, X. Pan, W. Yang, L. Mai, *Adv. Mater.* **2017**, *29*, 1604464; c) H. Wang, Z. Lu, S. Xu, D. Kong, J. J. Cha, G. Zheng, P.-C. Hsu, K. Yan, D. Bradshaw, F. B. Prinz, et al., *Proc. Natl. Acad. Sci. USA* **2013**, *110*, 19701–19706; d) C. Wan, Y. N. Regmi, B. M. Leonard, *Angew. Chem. Int. Ed.* **2014**, *53*, 6407–6410; *Angew. Chem.* **2014**, *126*, 6525–6528.
- [5] a) H. Li, M. Du, M. J. Mleczko, A. L. Koh, Y. Nishi, E. Pop, A. J. Bard, X. Zheng, *J. Am. Chem. Soc.* **2016**, *138*, 5123–5129; b) Y. Yin, J. Han, Y. Zhang, X. Zhang, P. Xu, Q. Yuan, L. Samad, X. Wang, Y. Wang, Z. Zhang, et al., *J. Am. Chem. Soc.* **2016**, *138*, 7965–7972.
- [6] K. Chang, X. Hai, H. Pang, H. Zhang, L. Shi, G. Liu, H. Liu, G. Zhao, M. Li, J. Ye, *Adv. Mater.* **2016**, *28*, 1–9.
- [7] D. Voiry, R. Fullon, J. Yang, E. S. C. de Carvalho Castro, R. Kappera, I. Bozkurt, D. Kaplan, M. J. Lagos, P. E. Batson, G. Gupta, et al., *Nat. Mater.* **2016**, *15*, 1003–1009.
- [8] a) H. P. Komsa, J. Kotakoski, S. Kurasch, O. Lehtinen, U. Kaiser, A. V. Krasheninnikov, *Phys. Rev. Lett.* **2012**, *109*, 035503; b) Y.-C. Lin, D. O. Dumcenco, Y.-S. Huang, K. Suenaga, *Nat. Nanotechnol.* **2014**, *9*, 391–396.
- [9] a) Y.-Y. Cai, X.-H. Li, Y.-N. Zhang, X. Wei, K.-X. Wang, J.-S. Chen, *Angew. Chem. Int. Ed.* **2013**, *52*, 11822–11825; *Angew. Chem.* **2013**, *125*, 12038–12041; b) H. Su, K.-X. Zhang, B. Zhang, H.-H. Wang, Q.-Y. Yu, X.-H. Li, M. Antonietti, J.-S. Chen, *J. Am. Chem. Soc.* **2017**, *139*, 811–818.
- [10] Z. H. Xue, H. Su, Q. Y. Yu, B. Zhang, H. H. Wang, X. H. Li, J. S. Chen, *Adv. Energy Mater.* **2017**, *7*, 1–7.
- [11] G. Akopov, M. T. Yeung, R. B. Kaner, *Adv. Mater.* **2017**, *29*, 1604506.
- [12] Y. Zheng, L. Lin, B. Wang, X. Wang, *Angew. Chem. Int. Ed.* **2015**, *54*, 12868–12884; *Angew. Chem.* **2015**, *127*, 13060–13077.
- [13] H. Wang, S. Jiang, S. Chen, D. Li, X. Zhang, W. Shao, X. Sun, J. Xie, Z. Zhao, Q. Zhang, et al., *Adv. Mater.* **2016**, *28*, 6940–6945.
- [14] a) J. K. Nørskov, T. Bligaard, A. Logadottir, J. R. Kitchin, J. G. Chen, S. Pandelov, U. Stimming, *J. Electrochem. Soc.* **2005**, *152*, J23; b) J. Kibsgaard, C. Tsai, K. Chan, J. D. Benck, J. K. Nørskov, F. Abild-Pedersen, T. F. Jaramillo, *Energy Environ. Sci.* **2015**, *8*, 3022–3029.
- [15] a) M. Huynh, C. Shi, S. J. L. Billinge, D. G. Nocera, *J. Am. Chem. Soc.* **2015**, *137*, 14887–14904; b) C. Kim, H. S. Jeon, T. Eom, M. S. Jee, H. Kim, C. M. Friend, B. K. Min, Y. J. Hwang, *J. Am. Chem. Soc.* **2015**, *137*, 13844–13850.
- [16] a) Q. Han, B. Wang, Y. Zhao, C. Hu, L. Qu, *Angew. Chem. Int. Ed.* **2015**, *54*, 11433–11437; *Angew. Chem.* **2015**, *127*, 11595–11599; b) Q. Liang, Z. Li, X. Yu, Z.-H. Huang, F. Kang, Q.-H. Yang, *Adv. Mater.* **2015**, *27*, 4634–4639.
- [17] J. Liu, Y. Liu, N. Liu, Y. Han, X. Zhang, H. Huang, Y. Lifshitz, S.-T. Lee, J. Zhong, Z. Kang, *Science* **2015**, *347*, 970–974.
- [18] a) H. Li, P. Wen, Q. Li, C. Dun, J. Xing, C. Lu, S. Adhikari, L. Jiang, D. L. Carroll, S. M. Geyer, *Adv. Energy Mater.* **2017**, *7*, 1700513; b) H. Park, Y. Zhang, J. P. Scheifers, P. R. Jothi, A. Encinas, B. P. T. Fokwa, *J. Am. Chem. Soc.* **2017**, *139*, 12915–12918; c) P. R. Jothi, Y. Zhang, J. P. Scheifers, H. Park, B. P. T. Fokwa, *Sustainable Energy Fuel* **2017**, *1*, 1928–1934.

Manuscript received: August 24, 2017

Revised manuscript received: October 24, 2017

Accepted manuscript online: November 8, 2017

Version of record online: December 7, 2017